

Exciton band topology in spontaneous quantum anomalous Hall insulators: applications to twisted bilayer graphene

Yves H. Kwan,¹ Yichen Hu,¹ Steven H. Simon,¹ and S. A. Parameswaran¹

¹*Rudolf Peierls Centre for Theoretical Physics, Clarendon Laboratory, Oxford OX1 3PU, UK*
(Dated: April 2, 2021)

We uncover topological features of neutral particle-hole pair excitations of correlated quantum anomalous Hall (QAH) insulators whose approximately flat conduction and valence bands have equal and opposite non-zero Chern number. Using an exactly solvable model we show that the underlying band topology affects both the center-of-mass and relative motion of particle-hole bound states. This leads to the formation of topological exciton bands whose features are robust to nonuniformity of both the dispersion and the Berry curvature. We apply these ideas to recently-reported broken-symmetry spontaneous QAH insulators in substrate aligned magic-angle twisted bilayer graphene.

Introduction.—The structure of the ground states of condensed matter systems intricately affects their low-temperature properties, and is imprinted in the spectrum of low-energy quasiparticles and long-wavelength collective excitations. Electrical insulators generically break no continuous symmetries and hence lack gapless collective modes, and are gapped to charge transport in their bulk. However, interactions can stabilize neutral excitons, bound states of a hole in the valence band and an electron in the conduction band. While also gapped, excitons typically have lower energy than charged excitations and dominate the optical response of direct-gap semiconductors, where they can be excited at zero wavevector. More generally, excitons form at a fixed ‘center of mass’ (CM) wavevector \mathbf{q} set by the momentum separation between the valence band maximum and conduction band minimum. The spectrum and transport properties of excitons can also be modified by the topology of the electronic bands near these extrema [1, 2]. This is captured by the *excitonic* Berry curvature [3] linked to the evolution of the two-particle bound state across its Brillouin zone (BZ). Such considerations are relevant, for example, to two-dimensional transition-metal dichalcogenides [4], where the valley-contrasting anomalous velocity of excitons has been experimentally observed [5].

Here, we focus on excitons in correlated insulators formed in moiré heterostructures of twisted bilayer graphene (TBG) aligned with hexagonal boron nitride (hBN). In the ‘magic angle’ regime, absent interactions, the relevant band structure has a gapped Dirac dispersion with four degenerate bands below and above charge neutrality [6, 7]. Members of each degenerate quartet are labeled by spin ($\sigma = \uparrow, \downarrow$) and valley ($\tau = \pm$) indices. The valleys correspond to the $\pm K$ points of the single-layer BZ, have Chern numbers $C = \tau$, and are interchanged by time-reversal symmetry (TRS). At integer filling, the suppressed bandwidth ($\lesssim 10$ meV) allows interactions to stabilize TRS-breaking valley- and spin-polarized states in which a partial subset of the bands is fully occupied — a mechanism proposed to explain the observed quantized anomalous Hall (QAH) response in hBN-TBG [8].

We identify several striking features of the exciton spectrum in hBN-TBG linked to the flatness and non-trivial Chern number of the underlying single-particle bands coupled with the spontaneous breaking of time-reversal and spin rotation symmetries. We root our understanding of universal topological features in an analytically tractable model that mimics the features of the hBN-TBG band structure by leveraging the mapping between $|C| = 1$ Chern bands and Landau levels (LLs). Our four-band model has perfectly flat dispersion and uniform Berry curvature, and consists of spinful electron LLs whose Chern number has a sign set by a two-fold degenerate valley index. We examine excitations of a fully spin-and-valley-polarized state with one filled LL. We show that the intravalley spin-wave mode has the gapless quadratic dispersion expected for Goldstone modes of a conserved order parameter, consistent with closely related quantum Hall ferromagnets [9, 10]. In striking contrast, we show that the intervalley excitonic bands of our model are gapped and exactly flat. The flatness of the bands admits low-energy $\mathbf{q} = 0$ excitons throughout the BZ, and also leads us to consider the dynamics of the excitonic CM which is conjugate to \mathbf{q} . Strikingly, we find that the CM motion experiences significant anomalous velocity, linked to the Berry curvature of the evolution of the particle-hole (PH) pair wavefunction as \mathbf{q} evolves across the CM. We demonstrate that these qualitative features survive the introduction of finite bandwidth and Berry curvature inhomogeneity, and discuss the results in a microscopic model of hBN-TBG. Our work illustrates that correlated ground states in moiré heterostructures can host unconventional excitations, whose many-body physics we explore elsewhere [11].

Exactly solvable model.— We exploit the topological equivalence between $|C| = 1$ Chern bands and LLs, and consider a system of four flavors of electronic LLs confined to the plane (Fig. 1a). The two valleys $\tau = \pm$ experience opposite magnetic fields $\mathbf{B} = -\tau B \hat{z}$, chosen to model the Chern band structure of TBG, and we neglect Zeeman splitting since there is no *real* external magnetic field. In Landau gauge $\mathbf{A}_\tau = -\tau B x \hat{y}$, the lowest Landau

level (LLL) wavefunctions are $\phi_{k\tau}(\mathbf{r}) \propto e^{iky} e^{-\frac{(x-\tau k)^2}{2}}$, which are created by $c_{k\tau\sigma}^\dagger$. We take $\ell_B \equiv (\hbar/eB)^{1/2} = 1$ throughout. The projected LLL Hamiltonian is [12]

$$\hat{H} = \frac{1}{2} \sum_{\substack{kpq \\ \tau\tau'\sigma\sigma'}} V_{\tau\tau'}(k, p, q) c_{k+q, \tau\sigma}^\dagger c_{k+p-q, \tau'\sigma'}^\dagger c_{k+p, \tau'\sigma'} c_{k, \tau\sigma} - \sum_{kp\tau\sigma} V_{\tau+}(k, p, 0) c_{k\tau\sigma}^\dagger c_{k\tau\sigma} + \text{const.}, \quad (1)$$

where the second line is a uniform background charge (equivalent to a filled $\tau = +$ LL), and $U(r) = e^2/r$ describes Coulomb interactions with LLL matrix elements $V_{\tau\tau'}(k, p, q) \equiv \langle k+q, \tau; k+p-q, \tau' | \hat{U} | k, \tau; k+p, \tau' \rangle$. The form of (1) is motivated by TBG, where interactions have $SU(2)$ spin rotation invariance and the suppressed intervalley scattering contributions are neglected [6].

We consider a uniform fully spin- and valley-polarized ground state, assuming without loss of generality that $(\tau, \sigma) = (+, \uparrow)$, viz. $|G\rangle \equiv \prod_k c_{k+\uparrow}^\dagger |vac\rangle$. The scenario with three filled flavors is equivalent via PH conjugation. Following Ref. [12], we compute the collective mode spectrum in the time-dependent Hartree-Fock approximation (TDHFA, equivalent to the generalized random phase approximation [13]). To do so, we solve the dynamics restricted to the basis of single PH pairs, created by the neutral operators $b_{\tau\sigma}^\dagger(k, q) \equiv c_{k+q, \tau\sigma}^\dagger c_{k, +\uparrow}$ (where q is the momentum transfer) that satisfy the equation of motion

$$-i\partial_t b_{\tau\sigma}^\dagger(k, q) = (\epsilon_{\tau\sigma}^{\text{HF}}(k+q) - \epsilon_{+\uparrow}^{\text{HF}}(k)) b_{\tau\sigma}^\dagger(k, q) - \sum_{k'} V_{\tau+}(k+q, k'-k-q, k'-k) b_{\tau\sigma}^\dagger(k', q), \quad (2)$$

where $(\tau, \sigma) \neq (+, \uparrow)$, and the k -independent Hartree-Fock (HF) energies are $\epsilon_{\tau\sigma}^{\text{HF}} = -\delta_{\sigma\uparrow} \delta_{\tau+} \sum_p V_{++}(\cdot, p, p)$. Eq. (2) is closed for a given τ, σ , and q as these are conserved by the Hamiltonian. Thus, TDHFA is *exact* for the one PH subspace when we neglect LL mixing.

We solve (2) by finding operators $\gamma_{\tau\sigma}^\dagger(q) = \int dk \psi_{q\tau\sigma}(k) b_{\tau\sigma}^\dagger(k, q)$ such that to leading order in $\gamma_{\tau\sigma}(q)$ $[\hat{H}, \gamma_{\tau\sigma}^\dagger(k)] = \omega_{\tau\sigma}(q) \gamma_{\tau\sigma}^\dagger(k)$, where $\omega_{\tau\sigma}(q)$ is the excitation energy. The coefficients $\psi_{q\tau\sigma}(k)$ satisfy

$$(U^{\text{HF}} - \omega_{\tau\sigma}(q)) \psi_{q\tau\sigma}(k) = \int dk' T_{q,\tau}(k, k') \psi_{q\tau\sigma}(k'), \quad (3)$$

with kernel $T_{q,\tau}(k, k') = \frac{L_y}{2\pi} V_{\tau+}(k'+q, k-k'-q, k-k')$, where $U^{\text{HF}} = \sqrt{\frac{\pi}{2}} \frac{e^2}{\ell_B}$. Discretizing Eq. (3) yields a 1D hopping problem for each q , with matrix element $T_{q,\tau}(k, k')$ between sites k, k' .

Intravalley spin-wave mode.— For $(\tau, \sigma) = (+, \downarrow)$ and fixed q , the hopping kernel $T_{q,\tau}(k, k')$ depends only on $k - k'$. With the ansatz $\psi_{q\tau\sigma}(k) \sim e^{ik\alpha}$ [12], the energy of this spin wave collective mode is given by [9, 10]

$$\omega_{+\downarrow}(q, \alpha) = U^{\text{HF}} - \int dk e^{ik\alpha} V_{++}(\cdot, k-q, k), \quad (4)$$

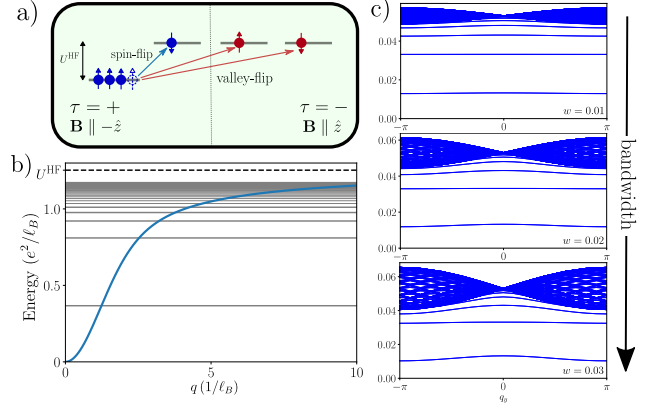


FIG. 1. (a) Schematic of the four-band LLL model at $\nu = 1$ showing the exchange-splitting $U^{\text{HF}} = \sqrt{\frac{\pi}{2}} \frac{e^2}{\ell_B}$ and the different neutral excitation types. (b) Spin wave energy (blue curve) as a function of y -momentum q for $\alpha = 0$. Horizontal lines show the momentum-independent valley-flip exciton energies. Both modes saturate to U^{HF} . (c) Intervalley exciton spectrum at $q_x = 0$ in the magnetic Brillouin with increasing bandwidth $w = 0.01, 0.02, 0.03$. Calculations were performed on a 20×20 momentum-space mesh.

plotted in Fig. 1a. The dispersion is isotropic in the (q, α) plane, and α can be interpreted as the x -momentum [12]. $\omega_{+\downarrow}(q)$ is gapless and quadratic for $q \rightarrow 0$ [9, 10, 14] and as $q \rightarrow \infty$ it saturates to U^{HF} (the loss of exchange energy in creating a hole) since in this limit electron and hole are sufficiently distant that their Coulomb energy vanishes.

Intervalley exciton mode.— A more interesting case is that of intervalley excitations where $\tau = -$. The spectrum is spin-independent since \hat{H} is $SU(2)$ -symmetric. In fact, the spectrum $\omega_{-\sigma}(q)$ is also independent of q , and hence macroscopically degenerate — a consequence of the ‘shift symmetry’ of the kernel, $T_{q,-}(k, k') = T_{q+2\delta,-}(k-\delta, k'-\delta)$ [15], where increasing q by δ corresponds to shifting the effective 1D hopping problem by $-\delta/2$. The sign and the factor of two is strongly suggestive of the notion that $b_{\tau\sigma}^\dagger(k, q)$ creates an excitation that couples to the magnetic field with an effective strength $2eB$ (recall the position-momentum locking of LLLs, $\langle x \rangle = \tau k \ell_B^2$). This leads to a discrete q -independent spectrum of excitonic bound states (Fig. 1a) described by harmonic oscillator wavefunctions $\psi_{q\tau\sigma}(k; n) \propto H_n[\sqrt{2}(k + \frac{q}{2})] e^{-(k + \frac{q}{2})^2}$ centered at $-q/2$, where H_n is a Hermite polynomial corresponding to LLLs in an effective magnetic field $2B$.

For rotationally invariant interactions we can capture key features of the excitons [11, 15] by working in symmetric gauge and performing a PH transformation on the $\tau = +$ valley, yielding a two-body Hamiltonian for the $+$ hole and $-$ electron. The CM sector is a LLL problem for a charge $-2e$ particle in $-B\hat{z}$, yielding a macroscopic degeneracy $N_{\text{exc}} = 2N_\Phi$ of each valley-flip level due to the

doubled coupling to the field. The relative motion corresponds to a charge $-e/2$ particle in the same field and a Coulomb central potential. Solving this in terms of Haldane pseudopotentials [16] yields discrete exciton binding energies $E_m = -\frac{e^2}{\ell_B} \frac{\Gamma(m+\frac{1}{2})}{2\Gamma(m+1)}$ (where $m \geq 0$ is an integer and Γ is the gamma function), in agreement with numerical solution of Eq. (3). The exciton is a composite neutral object which sees an effectively doubled magnetic field, and whose CM and relative motion are topologically non-trivial (due to Landau quantization) for any interaction. Semiclassical quantization also gives a macroscopic CM degeneracy and discrete relative energy levels, because of the Lorentz-force deflection of electrons and holes as they attract in opposing magnetic fields. In contrast, for the usual case of identical fields the CM of the PH pair evolves in zero field and its energy is non-degenerate [17].

Perturbations away from the LL limit.— We are interested in studying Chern bands with small but non-zero dispersion and non-uniform Berry curvature. To model effects of the single-particle dispersion in our LL model, we transform to the magnetic Bloch basis indexed by two-dimensional momenta \mathbf{k} in the magnetic BZ. Picking a square unit cell with side $a = \sqrt{2\pi}$ enclosing unit flux (for magic-angle TBG with $a \simeq 14$ nm, this corresponds to $B \simeq 5$ T), the single-particle magnetic Bloch operators are [6] $d_{\mathbf{k}\tau}^\dagger = \frac{1}{\sqrt{N_x}} \sum_{n=0}^{N_x-1} e^{i\tau k_x(k_y+nQ)} c_{k_y+nQ,\tau}^\dagger$ where $Q = \frac{2\pi}{a}$ is the BZ length and the spin index has been dropped as we are focusing on intervalley modes. Following Ref. [6] we introduce a potential $V(\mathbf{r}) = -w(\cos(\frac{2\pi x}{a}) + \cos(\frac{2\pi y}{a}))$, which is diagonal in this basis and projects to a single-particle dispersion $\epsilon_{\mathbf{k}} = -we^{-\frac{\pi}{2}}(\cos k_x a + \cos k_y a)$ in the LL. Solving the discretized TDHFA equations, we find that exciton energies evolve with the CM momenta \mathbf{q} , forming bands within the BZ (Fig. 1c). The topology of exciton bands is encoded in their Berry curvature [3], as we now summarize [15]. The exciton state is [18]

$$|\psi_{\mathbf{q}}^{\text{exc}}\rangle = \sum_{\mathbf{k}} \psi_{\mathbf{q}}(\mathbf{k}) d_{\mathbf{k}+\frac{\mathbf{q}}{2},-}^\dagger d_{\mathbf{k}-\frac{\mathbf{q}}{2},+} |G\rangle. \quad (5)$$

After PH-transforming the + valley, we can write

$$|u_{\mathbf{q}}^{\text{exc}}\rangle = e^{-i\mathbf{q}\hat{\mathbf{R}}} \sum_{\mathbf{k}} \psi_{\mathbf{q}}(\mathbf{k}) |\phi_{\mathbf{k}+\frac{\mathbf{q}}{2},-}\rangle |\phi_{\mathbf{k}-\frac{\mathbf{q}}{2},+}^*\rangle, \quad (6)$$

where $|\phi_{\mathbf{k},\tau}\rangle$ are the single-particle Bloch states, and the $e^{-i\mathbf{q}\hat{\mathbf{R}}}$ prefactor ensures that the cell-periodic part $|u_{\mathbf{q}}^{\text{exc}}\rangle$ of $|\psi_{\mathbf{q}}^{\text{exc}}\rangle$ satisfies \mathbf{q} -independent boundary conditions [19]. The Berry connection and gauge-invariant Berry curvature are then computed from $|u_{\mathbf{q}}^{\text{exc}}\rangle$. If $\mathbf{a}^\tau = i\langle u_{\mathbf{q}}^\tau | \nabla_{\mathbf{q}} | u_{\mathbf{q}}^\tau \rangle$ and $f^\tau = \nabla_{\mathbf{q}} \times \mathbf{a}_\tau(\mathbf{q})$ are the Berry connection and curvature of the underlying single-particle bands, the exciton Berry curvature takes the form

$$\Omega_{\text{exc}}(\mathbf{q}) = \Omega_{\text{sp}}(\mathbf{q}) + \Omega_e(\mathbf{q}) + \Omega_{\text{sp,e}}(\mathbf{q}), \quad (7)$$

where (defining $\mathbf{k}_\pm = \mathbf{k} \pm \frac{\mathbf{q}}{2}$) the first contribution

$$\Omega_{\text{sp}}(\mathbf{q}) = \frac{i}{4} \sum_{\mathbf{k}} |\psi_{\mathbf{q}}(\mathbf{k})|^2 \{f^+(\mathbf{k}_-) - f^-(\mathbf{k}_+)\} \quad (8)$$

stems from the single-particle Berry curvature,

$$\Omega_e(\mathbf{q}) = i \sum_{\mathbf{k}} \partial_{q_x} \psi_{\mathbf{q}}(\mathbf{k}) \partial_{q_y} \psi_{\mathbf{q}}^*(\mathbf{k}) - \partial_{q_y} \psi_{\mathbf{q}}(\mathbf{k}) \partial_{q_x} \psi_{\mathbf{q}}^*(\mathbf{k}) \quad (9)$$

captures the BZ evolution of the envelope function, and

$$\Omega_{\text{sp,e}}(\mathbf{q}) = \frac{i}{2} \sum_{\mathbf{k},\tau=\pm} \{\partial_{q_y} |\psi_{\mathbf{q}}(\mathbf{k})|^2 a_x^{-\tau}(\mathbf{k}_\tau) - (x \leftrightarrow y)\} \quad (10)$$

describes the coupling between the envelope function and the single-particle Berry connection. (Due to the ambiguity in defining \mathbf{a} and the phase of $\psi_{\mathbf{k}}(\mathbf{q})$, only the combination $\Omega_e + \Omega_{\text{sp,e}}$ is gauge-invariant.) Numerically $\Omega_{\text{exc}}(\mathbf{q})$ is computed on a finite k -mesh by computing gauge-invariant (non-Abelian) lattice field strengths [20]. Integrating $\Omega_{\text{exc}}(\mathbf{q})$ over the BZ gives a quantized exciton Chern number $C_{\text{exc}} = \int_{\text{BZ}} \frac{d^2 q}{2\pi} \Omega_{\text{exc}}(\mathbf{q})$.

Armed with this definition we return to our discussion of perturbing the solvable limit. At $w = 0$ the bands are flat and two-fold degenerate [22], consistent with the CM experiencing a doubled effective field. As the bandwidth is increased, the upper levels merge into a continuum, which engulfs additional bands as w grows (Fig. 1c). At large enough w the lowest exciton band dips below $E = 0$, signaling an instability to a partially-polarized state at the one-exciton level. We also introduce Berry curvature inhomogeneity by artificially deforming the Landau gauge states [15], and find that this leads to a weak exciton dispersion but preserves the Chern numbers. These results illustrate that the exciton dispersion arises from the interplay of the underlying band geometry, topology, dispersion, and interactions. We have also explicitly verified that low-lying exciton bands remain topological with $C_{\text{exc}} = 1$ under these perturbations, even as they acquire dispersion and Berry curvature fluctuations of their own.

Microscopic calculation in TBG.— We now turn to spin and valley-flip excitons of hBN-TBG, for which our starting point is the continuum model of Ref. [21] with twist $\theta \simeq 1.2^\circ$ lying in the magic angle regime. We choose the inter-layer couplings $w_{AA} = 0.08$ eV and $w_{AB} = 0.11$ eV to account for lattice relaxation effects [23, 24]. The hBN alignment is introduced via a sublattice splitting $|\Delta| = 20$ meV on the bottom layer. We use a dual-gate screened interaction $U(q) = \frac{e^2}{2\epsilon\epsilon_0 q} \tanh(qd_{\text{sc}})$ with relative permittivity $\epsilon = 9.5$ and screening length $d_{\text{sc}} = 40$ nm [25], and account for interaction double-counting by measuring the density relative to that of decoupled graphene sheets at charge neutrality [15, 26]. Projecting to the eight central bands for simplicity, we calculate the fully flavor-polarized self-consistent QAH state at the experimentally-relevant filling $\nu = +3$ [8], from which we compute the single valley-flip or spin-flip

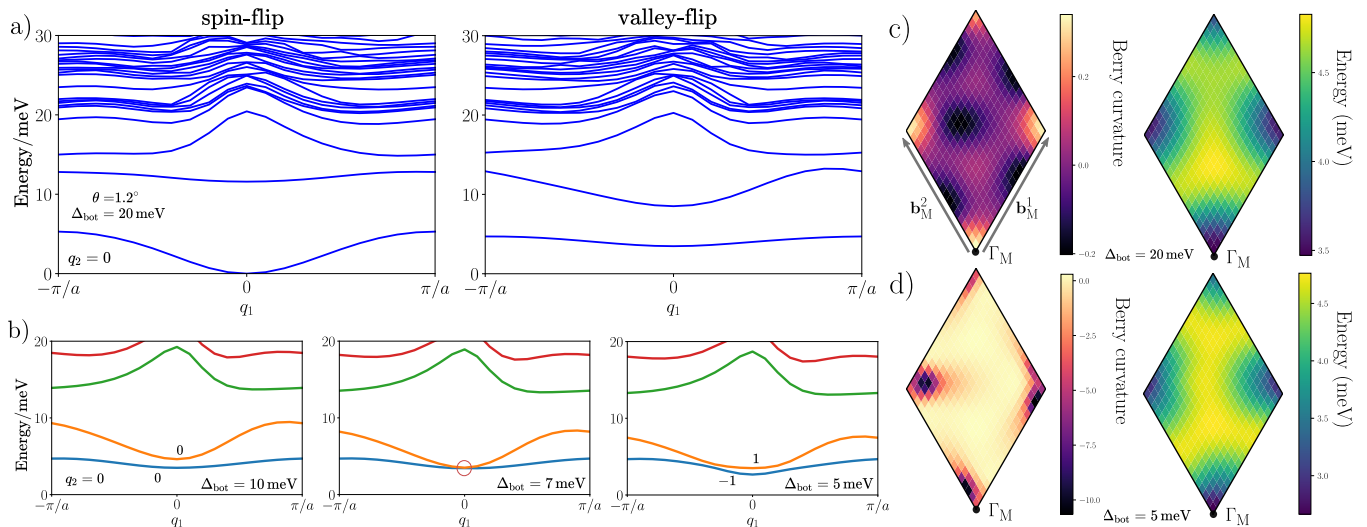


FIG. 2. (a) Spin- and valley-flip exciton spectrum of $\nu = +3$ QAH state of TBG using the continuum model [21], shown along the K_M - Γ_M - K_M line in the moiré BZ (mBZ). (b) As substrate potential is varied, intervalley exciton bands cross at Γ_M in a topological transition where the Chern numbers of the lowest bands change as indicated with $|\Delta C_{\text{exc}}| = 1$. (c) Berry curvature (multiplied by the moiré BZ area) and exciton energy for the lowest valley-flip band of (a) in the moiré BZ. The origin Γ_M and the reciprocal lattice vectors $\mathbf{b}_M^{1(2)} = \sqrt{3}k_\theta(\pm 1/2, \sqrt{3}/2)$ are indicated, where the moiré wavevector $k_\theta = \frac{8\pi}{3\sqrt{3}a} \sin \frac{\theta}{2}$. (d) Same as (c) but for the $C_{\text{exc}} = -1$ band of the final panel of (b). System size is 20×20 .

excitonic spectra in Fig. 2a [15]. Consistent with previous studies that focused on energetics [14, 27], we find that the spin-flip mode is gapless and disperses quadratically at zero momentum, while the valley-flip mode is gapped. The energetic separation and narrow bandwidth $\simeq 1$ meV of the lowest valley-flip exciton band (Fig. 2c) is promising for flat-band physics.

For the above parameters, we find that the lowest two exciton bands have $C_{\text{exc}} = 0$. We emphasize however that the physics of TBG shows large sample-to-sample variations sensitive to the precise device parameters and experimental conditions. Indeed, by varying the substrate strength, we can induce a set of band touching events which renders the lowest exciton band topological (Fig. 2b,d). This reveals that the different terms in Eq. (7) can give competing contributions to the exciton Berry curvature. Specifically, the non-trivial structure of the envelope function $\psi_{\mathbf{q}}(\mathbf{k})$ can render exciton bands trivial even if the underlying single-particle bands have equal and opposite Chern numbers and yield a nonzero gauge-invariant $\Omega_{\text{sp}}(\mathbf{q})$. Despite these subtleties, it seems likely that hBN-TBG and other spontaneous QAH systems can host low-lying topological exciton branches in realistic parameter regimes.

Discussion.— We have studied the properties of excitons constituted of particles and holes from bands with equal and opposite Chern numbers, focusing on the Berry curvature experienced by the exciton center-of-mass momentum as it evolves across the BZ. We first studied a solvable model and then showed that universal features

are stable to including finite dispersion and Berry curvature inhomogeneities. Using these insights, we analysed the topology of the low-lying exciton dispersion in hBN-TBG. For realistic interactions we find substantial exciton Berry curvature, integrating to a non-zero Chern number for the lowest exciton band in a subset of the explored parameter space.

As with other topological collective modes [28–30], a non-zero Chern number for a bulk exciton band indicates the presence of chiral exciton modes [31–33] localized at the boundary of the QAH domain, traversing the bulk gap to connect the band to one with a distinct Chern number. These modes allow unidirectional exciton transport, acting as chiral channels for valley charge, but only emerge in TBG for a narrow range of parameters. However, even when the lowest exciton band has $C_{\text{exc}} = 0$, we nevertheless find substantial curvature inherited from the underlying Chern bands (Fig. 2c). This can drive anomalous exciton transport in the bulk [3, 5]. Each valley-flip exciton of QAH systems such as hBN-TBG is associated with a $U(1)$ valley charge. Since the latter is to very good approximation conserved in these systems, excitons are likely long-lived. Direct optical addressing of these excitons is challenged by the momentum mismatch between the valleys; however, it may be possible to supply this ‘missing momentum’ from another source, e.g. phonons [34]. As conserved bosons in a flat topological band, these valley-flip excitons are a potential platform for engineering neutral bosonic quantum Hall states, a question that we address in a companion work [11].

Acknowledgments.— We thank N. Bultinck, G. Wagner, B. Lian, S.L. Sondhi, and M.P. Zaletel for useful discussions. We acknowledge support from the European Research Council (ERC) under the European Union Horizon 2020 Research and Innovation Programme (Grant Agreement No. 804213-TMCS) and from EPSRC grant EP/S020527/1. Statement of compliance with EPSRC policy framework on research data: This publication is theoretical work that does not require supporting research data.

-
- [1] A. Srivastava and A. m. c. Imamoğlu, *Phys. Rev. Lett.* **115**, 166802 (2015).
- [2] J. Zhou, W.-Y. Shan, W. Yao, and D. Xiao, *Phys. Rev. Lett.* **115**, 166803 (2015).
- [3] W. Yao and Q. Niu, *Phys. Rev. Lett.* **101**, 106401 (2008).
- [4] G. Wang, A. Chernikov, M. M. Glazov, T. F. Heinz, X. Marie, T. Amand, and B. Urbaszek, *Rev. Mod. Phys.* **90**, 021001 (2018).
- [5] M. Onga, Y. Zhang, T. Ideue, and Y. Iwasa, *Nature materials* **16**, 1193 (2017).
- [6] N. Bultinck, S. Chatterjee, and M. P. Zaletel, *Phys. Rev. Lett.* **124**, 166601 (2020).
- [7] Y.-H. Zhang, D. Mao, and T. Senthil, arXiv preprint arXiv:1901.08209 (2019).
- [8] M. Serlin, C. L. Tschirhart, H. Polshyn, Y. Zhang, J. Zhu, K. Watanabe, T. Taniguchi, L. Balents, and A. F. Young, *Science* **367**, 900 (2020), <https://science.sciencemag.org/content/367/6480/900.full.pdf>.
- [9] Y. A. Bychkov, S. V. Iordanskiĭ, and G. M. Éliashberg, *Soviet Journal of Experimental and Theoretical Physics Letters* **33**, 143 (1981).
- [10] C. Kallin and B. I. Halperin, *Phys. Rev. B* **30**, 5655 (1984).
- [11] Y. H. Kwan, Y. Hu, S. H. Simon, and S. A. Parameswaran, “Excitonic fractional quantum hall hierarchy in moiré heterostructures,” (2020), arXiv:2003.11559 [cond-mat.str-el].
- [12] A. Karlhede, K. Lejnell, and S. L. Sondhi, *Phys. Rev. B* **60**, 15948 (1999).
- [13] P. Nozieres and D. Pines, *Theory Of Quantum Liquids*, Advanced Books Classics (Avalon Publishing, 1999).
- [14] Y. Alavirad and J. Sau, *Phys. Rev. B* **102**, 235123 (2020).
- [15] See Supplemental Material for additional details of theoretical analyses and numerical calculations.
- [16] F. D. M. Haldane, *Phys. Rev. Lett.* **51**, 605 (1983).
- [17] L. P. Gor’kov and I. E. Dzyaloshinskiĭ, *Soviet Journal of Experimental and Theoretical Physics* **26**, 449 (1968).
- [18] The decomposition of the momenta into $\mathbf{k} \pm \frac{\mathbf{q}}{2}$ is required to properly decouple the relative and CM sectors.
- [19] R. Resta, *Journal of Physics: Condensed Matter* **12**, R107 (2000).
- [20] T. Fukui, Y. Hatsugai, and H. Suzuki, *Journal of the Physical Society of Japan* **74**, 1674 (2005), <https://doi.org/10.1143/JPSJ.74.1674>.
- [21] R. Bistritzer and A. H. MacDonald, *Proceedings of the National Academy of Sciences* **108**, 12233 (2011), <https://www.pnas.org/content/108/30/12233.full.pdf>.
- [22] For the simple cosine potential considered here, each pair of bands never fully detaches because $\epsilon_{\mathbf{k}} = \epsilon_{-\mathbf{k}}$.
- [23] N. N. T. Nam and M. Koshino, *Phys. Rev. B* **96**, 075311 (2017).
- [24] S. Carr, S. Fang, Z. Zhu, and E. Kaxiras, *Phys. Rev. Research* **1**, 013001 (2019).
- [25] N. Bultinck, E. Khalaf, S. Liu, S. Chatterjee, A. Vishwanath, and M. P. Zaletel, *Phys. Rev. X* **10**, 031034 (2020).
- [26] M. Xie and A. H. MacDonald, *Phys. Rev. Lett.* **124**, 097601 (2020).
- [27] F. Wu and S. Das Sarma, *Phys. Rev. Lett.* **124**, 046403 (2020).
- [28] R. Shindou, R. Matsumoto, S. Murakami, and J.-i. Ohe, *Phys. Rev. B* **87**, 174427 (2013).
- [29] T. Karzig, C.-E. Bardyn, N. H. Lindner, and G. Refael, *Phys. Rev. X* **5**, 031001 (2015).
- [30] A. V. Nalitov, D. D. Solnyshkov, and G. Malpuech, *Phys. Rev. Lett.* **114**, 116401 (2015).
- [31] F. Wu, T. Lovorn, and A. H. MacDonald, *Phys. Rev. Lett.* **118**, 147401 (2017).
- [32] Z. Gong, W. Luo, Z. Jiang, and H. Fu, *Scientific reports* **7**, 42390 (2017).
- [33] K. Chen and R. Shindou, *Phys. Rev. B* **96**, 161101 (2017).
- [34] I. V. Kukushkin, J. H. Smet, V. W. Scarola, V. Umansky, and K. von Klitzing, *Science* **324**, 1044 (2009).
- [35] Y. H. Kwan, G. Wagner, N. Chakraborty, S. H. Simon, and S. A. Parameswaran, “Domain wall competition in the chern insulating regime of twisted bilayer graphene,” (2020), arXiv:2007.07903 [cond-mat.str-el].
- [36] P. Ring and P. Schuck, *The nuclear many-body problem* (Springer Science & Business Media, 2004).

**SUPPLEMENTARY INFORMATION FOR “EXCITON BAND TOPOLOGY IN SPONTANEOUS
QUANTUM ANOMALOUS HALL INSULATORS: APPLICATIONS TO TWISTED BILAYER
GRAPHENE”**

Coulomb Matrix Elements

In this section we give expressions for the interaction matrix elements that enter the TDHFA equations for the collective modes of the lowest Landau levels in opposite fields. We define

$$\begin{aligned} V_{\tau_1\tau_2\tau_3\tau_4}(k, p, q) &\equiv \langle k + q, \tau_1; k + p - q, \tau_2 | \hat{U} | k, \tau_4; k + p, \tau_3 \rangle \\ &= \iint d\mathbf{r} d\mathbf{r}' U(\mathbf{r} - \mathbf{r}') \phi_{k+q, \tau_1}^*(\mathbf{r}) \phi_{k+p-q, \tau_2}^*(\mathbf{r}') \phi_{k+p, \tau_3}(\mathbf{r}') \phi_{k, \tau_4}(\mathbf{r}). \end{aligned} \quad (11)$$

where $U(\mathbf{r}) = e^2/|\mathbf{r}|$ and $\phi_{k, \tau}(\mathbf{r}) = \frac{1}{\sqrt{\pi^{\frac{1}{2}} L_y}} e^{iky} e^{-\frac{(x-\tau k)^2}{2}}$. After some work, this simplifies to

$$V_{\tau_1\tau_2\tau_3\tau_4}(k, p, q) = \frac{e^2}{L_y} \sqrt{\frac{2}{\pi}} \int_{-\infty}^{\infty} dx K_0(|qx|) e^{-\frac{1}{2}(x^2 + Bx + C)} \quad (12)$$

$$B = k(-\tau_1 + \tau_2 + \tau_3 - \tau_4) + p(\tau_2 + \tau_3) + q(-\tau_1 - \tau_2) \quad (13)$$

$$C = k^2 \left[4 - \frac{(\tau_1 + \tau_2 + \tau_3 + \tau_4)^2}{4} \right] + p^2 \left[2 - \frac{(\tau_2 + \tau_3)^2}{4} \right] + q^2 \left[2 - \frac{(\tau_1 - \tau_2)^2}{4} \right] \quad (14)$$

$$+ kp \left[4 - \frac{(\tau_2 + \tau_3)(\tau_1 + \tau_2 + \tau_3 + \tau_4)}{2} \right] + kq \left[-\frac{(\tau_1 + \tau_2 + \tau_3 + \tau_4)(\tau_1 - \tau_2)}{2} \right] \quad (15)$$

$$+ pq \left[-2 - \frac{(\tau_2 + \tau_3)(\tau_1 - \tau_2)}{2} \right], \quad (16)$$

where K_0 is a modified Bessel function of the second kind. We now focus on the cases of relevance to density-density interactions considered in the main text.

$$V_{++++}$$

This is the only matrix element that contributes to the pure spin flip excitation. Here, $B = 2(p - q)$ and $C = q^2 + (p - q)^2$. Clearly $V_{++++}(k, p, q)$ is independent of k —this makes sense because k is some overall momentum of the four states entering the matrix element, and this can always be removed by shifting the integrations of x, x' .

$$V_{-++-}$$

This appears in the direct Coulomb interaction between the constituent electron and hole of a intervalley exciton. Here, $B = 4k + 2p$ and $C = 4k^2 + p^2 + q^2 + 4kp$. From these coefficients we can deduce the very important property

$$V_{-++-}(k, p, q) = V_{-++-}(k + \delta, p - 2\delta, q). \quad (17)$$

This is satisfied for any interaction, not just Coulomb, and leads to the macroscopic degeneracy of each exciton energy level as explained in the main text.

Symmetric Gauge Calculation

In this section we analyze the valley-flip collective mode problem in the symmetric gauge, which is simpler due to the rotational invariance of the interaction. (Of course the Landau gauge is more suited to investigating the effects of a periodic potential.) It also has the advantage of being more natural from the perspective of finite-size considerations

(i.e. a Hall droplet). The single-particle states for the two valleys are

$$\chi_{m,+}(z) = \frac{A_m}{\sqrt{\pi}} z^m e^{-\frac{|z|^2}{4}} \quad (18)$$

$$\chi_{m,-}(z) = \frac{A_m}{\sqrt{\pi}} z^{*m} e^{-\frac{|z|^2}{4}} \quad (19)$$

$$A_m = (2^m m!)^{-\frac{1}{2}}, \quad (20)$$

and the Hamiltonian is (spin has been removed)

$$\hat{H} = \frac{1}{2} \sum_{m_1 m_2 n_1 n_2 \tau \tau'} V_{\tau\tau'}(n_1 n_2 m_2 m_1) c_{n_1 \tau}^\dagger c_{n_2 \tau'}^\dagger c_{m_2 \tau'} c_{m_1 \tau} \quad (21)$$

$$V_{\tau\tau'}(n_1 n_2 m_2 m_1) \equiv \int d\mathbf{r} d\mathbf{r}' U_{\tau\tau'}(\mathbf{r} - \mathbf{r}') \chi_{n_1, \tau}^*(z) \chi_{n_2, \tau'}^*(z') \chi_{m_2, \tau'}(z') \chi_{m_1, \tau}(z). \quad (22)$$

This is $(m_1, m_2) \rightarrow (n_1, n_2)$ scattering. Angular momentum conservation imposes selection rules that depend on the valleys involved. If $\tau = \tau'$, we have $n_1 + n_2 = m_1 + m_2$. If $\tau \neq \tau'$ we have $n_1 - n_2 = m_1 - m_2$. If the intervalley and intravalley interactions are the same, we have $V_{+-}(n_1 n_2 m_2 m_1) = V_{++}(n_1 m_2 n_2 m_1)$.

Let $|G\rangle = \prod_m c_{m+}^\dagger |\text{vac}\rangle$ be the reference ground state. The basis of single PH states will be parameterized as

$$|a, b\rangle \equiv c_{a,-}^\dagger c_{b,+} |G\rangle. \quad (23)$$

Here we will fix intervalley and intravalley interactions to be the same Coulomb form – assuming otherwise won't change the structure of the exciton states. From the selection rules, it is easy to see that $|0, 0\rangle$ is an exact eigenstate with energy above $|G\rangle$ of

$$E_{0,0} = \sum_n V_{++}(0n0n) - V_{+-}(0000) = \frac{e^2}{l_B} \left(\sqrt{\frac{\pi}{2}} - \frac{\sqrt{\pi}}{2} \right), \quad (24)$$

which matches the lowest exciton energy level described in the main text.

In fact from angular momentum conservation, the seed basis state $|n, 0\rangle$ only couples to $|n, 0\rangle, |n-1, 1\rangle, \dots, |0, n\rangle$. The matrix elements are $\langle n-l', l' | \hat{H}' | n-l, l \rangle = -V_{+-}(l, n-l', n-l, l')$, where the prime on \hat{H}' indicates deduction of the ground state energy.

Solving the finite-dimensional problem generated by $|n, 0\rangle$, we obtain the exciton binding energies in Eq. (32) for $m = 0, \dots, n$. Furthermore upon examination of the eigenvectors of the lowest exciton state, we find that the coefficients are consistent with a first-quantized wavefunction $\sim z^{*n} e^{-\frac{|u|^2}{8} - \frac{|z|^2}{2}}$ (Eq. (33)), independent of the form of the interaction potential (as long as the $m = 0$ pseudopotential is the largest one). This is consistent with the toy exciton calculation – projection of the CM to the LLL allows for a polynomial prefactor $f(z^*)$ in the CM coordinate.

The utility of doing the collective mode calculation in the symmetric gauge is that it provides a controlled way to count the degeneracy of exciton states as we approach the thermodynamic limit. For example, we can restrict ourselves to only allow particle-hole pairs whose components have angular momenta $\leq N$. Edge effects are apparent by considering say $|N, N\rangle$, for which there exist no other legal states to couple to. As $N \rightarrow \infty$ we expect to recover the physics of the bulk. Figure 3 shows that as N increases, the exciton degeneracy approaches $2N$ per energy level—this makes intuitive sense since the exciton has twice the coupling to the magnetic field, and therefore has twice as many states (per relative motion configuration).

Electron-hole Two-body Problem

Consider an electron and a hole with charges $-e$ and e respectively, and identical masses m . They are confined to the 2D $x-y$ plane, and are coupled to the vector potentials $\mathbf{A}_e = -\mathbf{A}_h = \mathbf{A}$, where the relative sign reflects the opposite magnetic fields felt by the two particles. They interact via an attractive potential $-v_d(r)$ with $v_d(r) > 0$, so that the Hamiltonian is

$$H_{\text{exc}} = \frac{(\mathbf{p}_e + e\mathbf{A})^2}{2m} + \frac{(\mathbf{p}_h + e\mathbf{A})^2}{2m} - v_d(r). \quad (25)$$

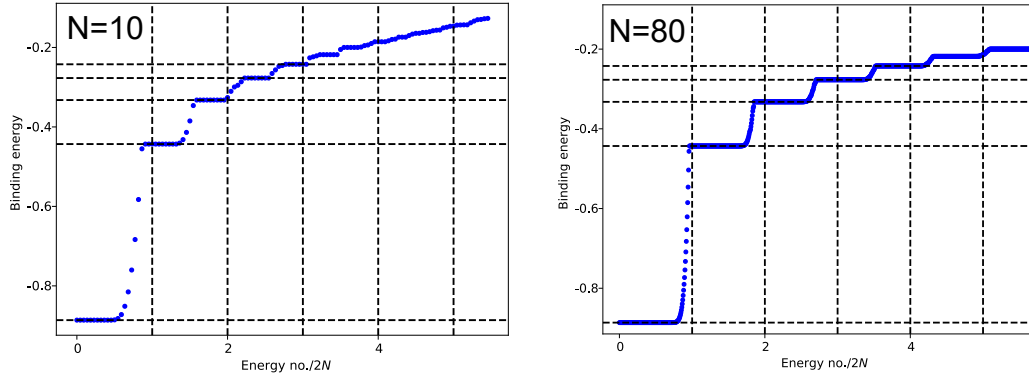


FIG. 3. Ordered valley flip exciton energies in units of $\frac{e^2}{\epsilon_B}$ for a system that only allows PH pairs whose components have angular momentum $\leq N$. The vertical dashed lines are spaced every $2N$, which is the expected exciton degeneracy as $N \rightarrow \infty$. The horizontal dashed lines are the expected bulk binding energies (Eq. (32)). We have zoomed in on the first ~ 5 exciton energy levels.

Now transform to centre-of-mass (CM) and relative coordinates

$$\mathbf{R} = \frac{\mathbf{r}_h + \mathbf{r}_e}{2}, \quad \mathbf{r} = \mathbf{r}_h - \mathbf{r}_e \quad (26)$$

$$\mathbf{P} = \mathbf{p}_h + \mathbf{p}_e, \quad \mathbf{p} = \frac{\mathbf{p}_h - \mathbf{p}_e}{2}. \quad (27)$$

In this basis, the Hamiltonian cleanly decouples into CM and relative sectors

$$H_{\text{exc}} = H_{\mathbf{R}} + H_{\mathbf{r}} \quad (28)$$

$$H_{\mathbf{R}} = \frac{(\mathbf{P} + 2e\mathbf{A})^2}{4m} \quad (29)$$

$$H_{\mathbf{r}} = \frac{(\mathbf{p} + \frac{e}{2}\mathbf{A})^2}{m} - v_d(r). \quad (30)$$

It will be most convenient to use the symmetric gauge $\mathbf{A} = \frac{B}{2}(-y\hat{x} + x\hat{y})$. The CM is a Landau level problem for particles of mass $2m$ and charge $-2e$ in a magnetic field B . This should be projected to the LLL, which provides the macroscopic degeneracy of the exciton energy levels. Owing to the increased coupling ($-2eB$) to the magnetic field, the degeneracy is $2N_{\Phi}$, twice that of the single-particle states.

On the other hand, the relative sector is mapped to a particle of mass $m/2$ and charge $-e/2$ in a magnetic field B , subject to an attractive central potential $-v_d(r)$. Upon projection to the LLL, $H_{\mathbf{r}}$ becomes easy to solve since the matrix elements of the potential are diagonal in the basis of LLL angular momentum eigenstates. Therefore the binding energies are simply Haldane pseudopotentials, and are obtained using symmetric gauge wavefunctions with magnetic length $\tilde{\ell}_B = \sqrt{2}\ell_B = \sqrt{2/eB}$

$$E_m = -\langle \psi_{LLL}^m | v_d(r) | \psi_{LLL}^m \rangle = -\frac{1}{2^{m-1}m!\tilde{\ell}_B^{2(m+1)}} \int dr v_d(r) r^{2m+1} e^{-\frac{r^2}{2\tilde{\ell}_B^2}}. \quad (31)$$

For the Coulomb interaction $v_d(r) = -e^2/r$, we obtain

$$E_m = -\frac{e^2}{\ell_B} \times \frac{\sqrt{\pi} (2m-1)!!}{2 \cdot 2^m m!}. \quad (32)$$

In terms of complex coordinates $z = \frac{z_h + z_e}{2}$ and $u = z_h - z_e$, the general form of an exciton eigenfunction in the m -th relative angular momentum channel is then

$$\psi_{\text{exc}}^m \sim \tilde{f}(z^*) u^m e^{-\frac{|z|^2}{2\ell_B^2}} e^{-\frac{|u|^2}{8\ell_B^2}} \quad (33)$$

where $\tilde{f}(z)$ is anti-analytic in z .

Magnetic Bloch Basis

In this section we construct the magnetic Bloch basis – this allows for an investigation into the effects of a periodic potential, as well as an explicit route to calculating the Berry curvature of the exciton bands. We take one flux per square unit cell $a^2 = 2\pi\ell_B^2 = 2\pi$. Following Ref. [6], the relation between the Landau gauge basis $c_{k,\tau}$ and the magnetic Bloch basis $d_{\mathbf{k},\tau}$ on a system of size $L_x = N_x a$, $L_y = N_y a$ is

$$d_{\mathbf{k},\tau}^\dagger = \frac{1}{\sqrt{N_x}} \sum_{n=-\frac{N_x}{2}}^{\frac{N_x}{2}-1} e^{i\tau k_x(k_y+nQ)} c_{k_y+nQ,\tau}^\dagger \quad (34)$$

$$c_{k_y+nQ,\tau}^\dagger = \frac{1}{\sqrt{N_x}} \sum_{k_x} e^{-i\tau k_x(k_y+nQ)} d_{\mathbf{k},\tau}^\dagger \quad (35)$$

$$k_x = \frac{2\pi n_{k_x}}{N_x a}, \quad n_{k_x} = 0, \dots, N_x - 1 \quad (36)$$

$$k_y = \frac{2\pi n_{k_y}}{N_y a}, \quad n_{k_y} = 0, \dots, N_y - 1. \quad (37)$$

where $Q = \frac{2\pi}{a} = a$ is the BZ side length.

The uniform Berry curvature of the SP states can be explicitly verified. The magnetic Bloch functions are

$$\psi_{\mathbf{k},\tau}(\mathbf{r}) = \frac{1}{\sqrt{N_x}} \sum_{n=-\frac{N_x}{2}}^{\frac{N_x}{2}-1} e^{i\tau k_x(k_y+nQ)} \phi_{k_y+nQ,\tau}(\mathbf{r}), \quad (38)$$

which obeys the boundary conditions appropriate for magnetic translations: $\psi_{\mathbf{k},\tau}(\mathbf{r} + a\hat{y}) = e^{ik_y a} \psi_{\mathbf{k},\tau}(\mathbf{r})$ and $\psi_{\mathbf{k},\tau}(\mathbf{r} + a\hat{x}) = e^{ik_x a} e^{i\tau Q y} \psi_{\mathbf{k},\tau}(\mathbf{r})$. The cell-periodic part is

$$u_{\mathbf{k},\tau}(\mathbf{r}) = e^{-i\mathbf{k}\mathbf{r}} \psi_{\mathbf{k},\tau}(\mathbf{r}) = \frac{1}{\sqrt{N_x L_y \pi^{\frac{1}{2}}}} \sum_n e^{i\tau k_x(k_y+nQ)} e^{-ik_x x} e^{inQy} e^{-\frac{[x-\tau(k_y+nQ)]^2}{2}}, \quad (39)$$

from which we may calculate the Berry connection and curvature

$$\mathbf{a}(\mathbf{k}) = -i \langle u(\mathbf{k}) | \partial_{\mathbf{k}} | u(\mathbf{k}) \rangle = (0, \tau k_x) \quad (40)$$

$$f = \partial_{k_x} a_y - \partial_{k_y} a_x = \tau. \quad (41)$$

Therefore the band of LLL magnetic Bloch states (as well as higher LLs) has Chern number $C = \tau$.

Interaction Hamiltonian

The position operator projected to the LLL is

$$\psi_\tau^\dagger(\mathbf{r}) = \frac{1}{\sqrt{L_y \pi^{\frac{1}{2}}}} \sum_k e^{-iky} e^{-\frac{1}{2}(x-\tau k)^2} c_{k\tau}^\dagger \quad (42)$$

$$k = \frac{2\pi n_k}{N_y a}, \quad k = -\frac{N_x}{2}, \dots, \frac{N_x}{2} - 1. \quad (43)$$

The number density operator in momentum space projected to the LLL is

$$n_\tau(\mathbf{q}) \equiv \int d\mathbf{r} e^{-i\mathbf{q}\mathbf{r}} \psi_\tau^\dagger(\mathbf{r}) \psi_\tau(\mathbf{r}) \quad (44)$$

$$= \int d\mathbf{r} e^{-i\mathbf{q}\mathbf{r}} \frac{1}{L_y \sqrt{\pi}} \sum_{k, k'} e^{i(k' - k)y - \frac{1}{2}(x - \tau k)^2 - \frac{1}{2}(x - \tau k')^2} c_{k\tau}^\dagger c_{k'\tau} \quad (45)$$

$$= \int dx e^{-iq_x x} \frac{1}{\sqrt{\pi}} \sum_k e^{-\frac{1}{2}(x - \tau k)^2 - \frac{1}{2}(x - \tau(k + q_y))^2} c_{k\tau}^\dagger c_{k + q_y, \tau} \quad (46)$$

$$= e^{-\frac{q^2}{4}} \sum_k e^{-iq_x \tau(k + \frac{q_y}{2})} c_{k\tau}^\dagger c_{k + q_y, \tau}. \quad (47)$$

We now rewrite this in terms of the magnetic Bloch operators

$$n_\tau(\mathbf{q}) = e^{-\frac{q^2}{4}} \frac{1}{N_x} \sum_{[k], n_k, k_x, k'_x} e^{-iq_x \tau([k] + n_k Q + \frac{q_y}{2})} e^{-i\tau k_x([k] + n_k Q)} e^{i\tau k'_x([k] + n_k Q + q_y)} d_{(k_x, [k])\tau}^\dagger d_{(k'_x, [k + q_y])\tau} \quad (48)$$

Where $[k]$ means $k \bmod Q$ which resides inside the 1BZ (which is defined here as the square with corners at $(0, 0)$ and (Q, Q)). We have used the decomposition $k = [k] + n_k Q$ where $n_k \in \mathbb{Z}$. Summing over n_k leads to $N_x \delta(k'_x = [q_x + k_x])$ since k'_x is in the 1BZ by definition. Then

$$n_\tau(\mathbf{q}) = e^{-\frac{q^2}{4}} \sum_{[k], k_x} e^{-iq_x \tau([k] + \frac{q_y}{2})} e^{-i\tau k_x [k]} e^{i\tau [q_x + k_x]([k] + q_y)} d_{(k_x, [k])\tau}^\dagger d_{([k_x + q_x], [k + q_y])\tau} \quad (49)$$

$$= e^{-\frac{q^2}{4}} \sum_{\mathbf{k} \in 1\text{BZ}} e^{i\tau(-q_x(k_y + \frac{q_y}{2}) - k_x k_y + [k_x + q_x](k_y + q_y))} d_{\mathbf{k}\tau}^\dagger d_{[\mathbf{k} + \mathbf{q}]\tau}. \quad (50)$$

The interaction Hamiltonian is

$$\hat{H}_{\text{int}} = \frac{1}{2} \sum_{\tau\tau'} \int d\mathbf{r} d\mathbf{r}' U_{\tau\tau'}(\mathbf{r} - \mathbf{r}') \psi_\tau^\dagger(\mathbf{r}) \psi_{\tau'}^\dagger(\mathbf{r}') \psi_{\tau'}(\mathbf{r}') \psi_\tau(\mathbf{r}) \quad (51)$$

$$= \frac{1}{2A} \sum_{\mathbf{q} \in \text{all}} \tilde{U}_{\tau\tau'}(\mathbf{q}) : n_\tau(-\mathbf{q}) n_{\tau'}(\mathbf{q}) : \quad (52)$$

with $A = L_x L_y$ the area. Summation over τ, τ' is implied. We substitute the density operators below. In the second equality, we split $\mathbf{q} \in \text{all}$ into a piece $\mathbf{q} \in 1\text{BZ}$ and a reciprocal lattice vector \mathbf{G} , and define $\mathbf{Q} \equiv \mathbf{q} + \mathbf{G}$ (this should not be confused with $Q = \frac{2\pi}{a}$)

$$\hat{H}_{\text{int}} = \frac{1}{2A} \sum_{\mathbf{q} \in \text{all}} \sum_{\mathbf{k}, \mathbf{k}' \in 1\text{BZ}} \tilde{U}_{\tau\tau'}(\mathbf{q}) e^{-\frac{q^2}{2}} e^{i\tau(q_x(k_y - \frac{q_y}{2}) - k_x k_y + [-q_x + k_x](k_y - q_y))} e^{i\tau'(-q_x(k'_y + \frac{q_y}{2}) - k'_x k'_y + [q_x + k'_x](k'_y + q_y))} \quad (53)$$

$$\times d_{\mathbf{k}\tau}^\dagger d_{\mathbf{k}'\tau'}^\dagger d_{[\mathbf{k}' + \mathbf{q}]\tau'} d_{[\mathbf{k} - \mathbf{q}]\tau} \quad (54)$$

$$= \frac{1}{2A} \sum_{\mathbf{k}, \mathbf{k}' \in 1\text{BZ}} \sum_{\mathbf{G}} \tilde{U}_{\tau\tau'}(\mathbf{Q}) e^{-\frac{Q^2}{2}} e^{i\tau(Q_x(k_y - \frac{Q_y}{2}) - k_x k_y + [-q_x + k_x](k_y - Q_y))} e^{i\tau'(-Q_x(k'_y + \frac{Q_y}{2}) - k'_x k'_y + [q_x + k'_x](k'_y + Q_y))} \quad (55)$$

$$\times d_{\mathbf{k}\tau}^\dagger d_{\mathbf{k}'\tau'}^\dagger d_{[\mathbf{k}' + \mathbf{q}]\tau'} d_{[\mathbf{k} - \mathbf{q}]\tau} \quad (56)$$

$$\equiv \frac{1}{2} \sum_{\mathbf{k}, \mathbf{k}' \in 1\text{BZ}} F_{\tau\tau'}(\mathbf{k}, \mathbf{k}', \mathbf{q}) d_{\mathbf{k}\tau}^\dagger d_{\mathbf{k}'\tau'}^\dagger d_{[\mathbf{k}' + \mathbf{q}]\tau'} d_{[\mathbf{k} - \mathbf{q}]\tau} \quad (57)$$

Relabelling momenta, we obtain

$$\hat{H}_{\text{int}} = \frac{1}{2} \sum_{\mathbf{k}, \mathbf{p}, \mathbf{q} \in 1\text{BZ}} M_{\tau\tau'}(\mathbf{k}, \mathbf{p}, \mathbf{q}) d_{[\mathbf{k} + \mathbf{q}]\tau}^\dagger d_{[\mathbf{k} + \mathbf{p} - \mathbf{q}]\tau'}^\dagger d_{[\mathbf{k} + \mathbf{p}]\tau} d_{\mathbf{k}\tau} \quad (58)$$

$$M_{\tau\tau'}(\mathbf{k}, \mathbf{p}, \mathbf{q}) = F_{\tau\tau'}([\mathbf{k} + \mathbf{q}], [\mathbf{k} + \mathbf{p} - \mathbf{q}], \mathbf{q}) \quad (59)$$

$$F_{\tau\tau'}(\mathbf{k}, \mathbf{k}', \mathbf{q}) \equiv \frac{1}{A} \sum_{\mathbf{G}} \tilde{U}_{\tau\tau'}(\mathbf{Q}) e^{-\frac{Q^2}{2}} e^{i\tau(Q_x(k_y - \frac{Q_y}{2}) - k_x k_y + [-q_x + k_x](k_y - Q_y))} e^{i\tau'(-Q_x(k'_y + \frac{Q_y}{2}) - k'_x k'_y + [q_x + k'_x](k'_y + Q_y))} \quad (60)$$

For an initial state $|G\rangle$ fully polarized in $\tau = +$, the TDHFA equations for the collective mode $|\text{exc}, \mathbf{q}\rangle = \psi_{\mathbf{q}}(\mathbf{k})d_{[\mathbf{k}+\mathbf{q}],-}^\dagger d_{\mathbf{k},+} |G\rangle$ are then

$$\omega_n(\mathbf{q})\psi_{q_n}(k) = \sum_{\mathbf{p}} M_{++}(\mathbf{k}, \mathbf{p}, \mathbf{p})\psi_{q_n}(\mathbf{k}) - \sum_{\mathbf{k}'} M_{\tau+}([\mathbf{k}' + \mathbf{q}], [\mathbf{k} - \mathbf{k}' - \mathbf{q}], [\mathbf{k} - \mathbf{k}'])\psi_{q_n}(\mathbf{k}') \quad (61)$$

$$= \sum_{\mathbf{p}} F_{++}([\mathbf{k} + \mathbf{p}], \mathbf{k}, \mathbf{p})\psi_{q_n}(\mathbf{k}) - \sum_{\mathbf{k}'} F_{\tau+}([\mathbf{k} + \mathbf{q}], \mathbf{k}', [\mathbf{k} - \mathbf{k}'])\psi_{q_n}(\mathbf{k}') \quad (62)$$

where n is the band index.

Berry Curvature of Valley-flip Exciton Bands

In the language of the magnetic Bloch basis, we can analytically compute the Berry curvature of the valley-flip exciton, since we know the analytical form of the envelope wavefunction. Recall the form of the exciton creation operator $\gamma_{q,m}^\dagger$ for the m -th degenerate exciton level in the Landau gauge

$$\gamma_{q,m}^\dagger = \int dk \psi_{q,m}(k) b^\dagger(k, q) \quad (63)$$

$$b^\dagger(k, q) = c_{k+q,-}^\dagger c_{k,+} \quad (64)$$

$$\psi_{q,m}(k) \propto H_m[\sqrt{2}(k + \frac{q}{2})] e^{-(k+\frac{q}{2})^2} = \tilde{\psi}_m(k + \frac{q}{2}) \quad (65)$$

where H_m is the m -th Hermite polynomial. $\tilde{\psi}(k)$ is centered at the origin with mean zero. Now consider following magnetic Bloch operator for the exciton

$$\Gamma_{\mathbf{q},m}^\dagger \equiv \frac{1}{\sqrt{N_x}} \sum_n \gamma_{q_y+2nQ,m}^\dagger e^{-\frac{iq_x}{2}(q_y+2nQ)} \quad (66)$$

whose wavefunction is (after performing a PH transformation in the $\tau = +$ band)

$$\psi_{\mathbf{q},m}^{\text{exc}}(\mathbf{r}_e, \mathbf{r}_h) = \frac{1}{\sqrt{N_x}} \sum_n \int dk \tilde{\psi}_m(k) e^{-\frac{iq_x}{2}(q_y+2nQ)} \phi_{k+\frac{q_y}{2}+nQ,-}(\mathbf{r}_e) \phi_{k-\frac{q_y}{2}-nQ,+}^*(\mathbf{r}_h). \quad (67)$$

To verify that this is the right candidate, we check the magnetic Bloch theorem by shifting the exciton CM coordinate $\mathbf{R} = \frac{\mathbf{r}_e + \mathbf{r}_h}{2}$

$$\psi_{\mathbf{q},m}^{\text{exc}}(\mathbf{r}_e + a\hat{x}, \mathbf{r}_h + a\hat{x}) = e^{-i(2Q)\frac{ye+yh}{2}} e^{iq_x a} \psi_{\mathbf{q},m}^{\text{exc}}(\mathbf{r}_e, \mathbf{r}_h) \quad (68)$$

$$\psi_{\mathbf{q},m}^{\text{exc}}(\mathbf{r}_e + \frac{a}{2}\hat{y}, \mathbf{r}_h + \frac{a}{2}\hat{y}) = e^{iq_y \frac{a}{2}} \psi_{\mathbf{q},m}^{\text{exc}}(\mathbf{r}_e, \mathbf{r}_h). \quad (69)$$

In the first line, the factor of two in the phase $e^{-i(2Q)\frac{ye+yh}{2}}$ reflects the fact that the exciton has twice the coupling to the magnetic field (compare with the SP case earlier). Therefore, the magnetic unit cell shrinks by a factor of two in the y -direction, so that the magnetic BZ of the exciton doubles in area.

The ‘cell-periodic’ part of the Bloch function is $u_{\mathbf{q}}^{\text{exc}}(\mathbf{r}_e, \mathbf{r}_h) = \exp(-i\mathbf{q} \cdot \frac{\mathbf{r}_e + \mathbf{r}_h}{2}) \psi_{\mathbf{q}}^{\text{exc}}(\mathbf{r}_e, \mathbf{r}_h)$, and we can straightforwardly compute the Berry connections

$$-i \langle u_{\mathbf{q}} | \partial_{q_x} | u_{\mathbf{q}} \rangle = 0, \quad -i \langle u_{\mathbf{q}} | \partial_{q_y} | u_{\mathbf{q}} \rangle = -\frac{q_x}{2} \quad (70)$$

leading to a curvature $f_{xy} = -\frac{1}{2}$. Integrated over the doubled magnetic BZ, this leads to $C = -1$.

Periodic Potential

Consider applying a potential $V_p(x, y)$ that is periodic in the square lattice. This enters the Hamiltonian as

$$\hat{H}_\tau^{\text{SP}} = \int d\mathbf{r} V_p(x, y) \psi_\tau^\dagger(\mathbf{r}) \psi_\tau(\mathbf{r}). \quad (71)$$

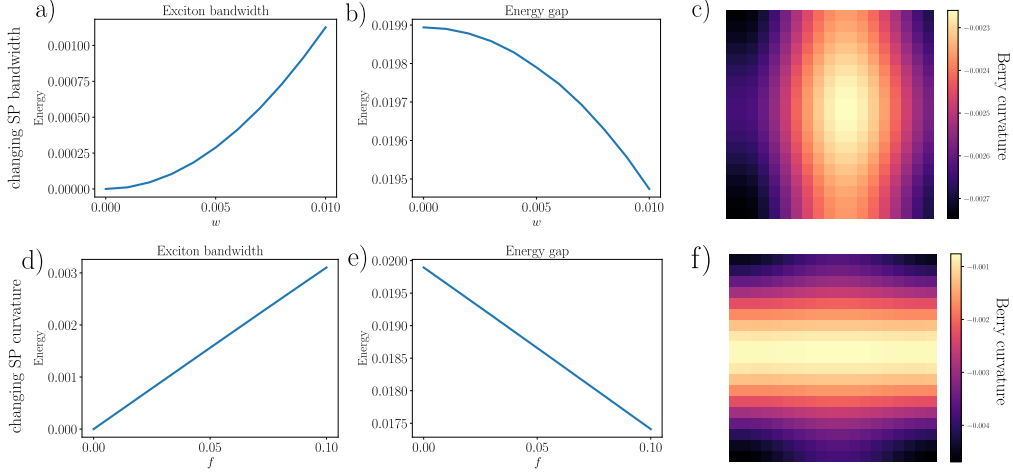


FIG. 4. a) Bandwidth of lowest exciton band with as a function SP bandwidth parameterized by w . The SP potential is chosen as $V_p(x, y) = -w(\cos(\frac{2\pi x}{a}) + \cos(\frac{2\pi y}{a}))$. b) Band gap between the first and second exciton bands with w . c) Berry curvature (normalized so that the mBZ sum over all cells is quantized in units of 2π) at $w = 0.005$. d-f) Same as a-c) except that the parameter being changed is the curvature of the underlying SP bands. The distortion of the bands used is $w(k_y) = f \sin(k_y/Q)$.

Note that we restrict ourselves to identical potentials on both valleys, to preserve the time-reversal relation between the two. Since we are in the LLL, any periodic potential is diagonal in the magnetic Bloch basis. In particular, harmonics of the potential are mapped to the following dispersions

$$\cos\left(\frac{2\pi n_x x}{a} + \phi_x\right) \rightarrow \epsilon_{\mathbf{k}, \tau} = e^{-\frac{n_x^2 \pi}{2}} \cos(\tau n_x k_y a + \phi_x) \quad (72)$$

$$\cos\left(\frac{2\pi n_y y}{a} + \phi_y\right) \rightarrow \epsilon_{\mathbf{k}, \tau} = e^{-\frac{n_y^2 \pi}{2}} \cos(\tau n_y k_x a + \phi_y) \quad (73)$$

For the TDHFA, this perturbation will appear on the RHS of 61 as a diagonal contribution of $\epsilon_{[\mathbf{k}+\mathbf{q}], -} - \epsilon_{\mathbf{k}, +}$. In Fig. 4a-c, we have used the potential $V_p(x, y) = -w(\cos(\frac{2\pi x}{a}) + \cos(\frac{2\pi y}{a}))$. The effect of the potential is to induce dispersion in the previously flat bands, as well as to redistribute the exciton Berry curvature. However the bands are still topological for finite w .

Distorted Landau Level States

To introduce Berry curvature inhomogeneity, we consider distorting the Landau gauge eigenstates with a ‘wobble’ factor respecting the square lattice periodicity $w(\mathbf{k} + \mathbf{Q}) = w(\mathbf{k})$, and the time-reversal relation of the two valleys $w(-\mathbf{k}) = -w(\mathbf{k})$

$$\phi_{\mathbf{k}, \tau}(w; \mathbf{r}) = \frac{1}{\sqrt{L_y \pi^{\frac{1}{2}}}} e^{ik_y y} e^{-\frac{[x - \tau(\mathbf{k} + w(\mathbf{k}))]^2}{2}}. \quad (74)$$

From this the distorted magnetic Bloch can be defined in analogy to Eq. (38). This perturbs the uniform Berry curvature in the y -direction, as can be explicitly verified

$$\mathbf{a}(\mathbf{k}) = -i \langle u(w; \mathbf{k}) | \partial_{\mathbf{k}} | u(w; \mathbf{k}) \rangle = (-\tau w(k_y), \tau k_x) \quad (75)$$

$$f = \partial_{k_x} a_y - \partial_{k_y} a_x = \tau + \tau \partial_{k_y} w(k_y), \quad (76)$$

but leaves the Chern number unchanged at $C = \tau$.

The TDHFA equations are the same except that the interactions are altered such that F in Eq. (60) is replaced with

$$\begin{aligned}
F_{\tau\tau'}(\mathbf{k}, \mathbf{k}', \mathbf{q}) \equiv & \frac{1}{A} \sum_{\mathbf{G}} \tilde{U}_{\tau\tau'}(\mathbf{Q}) e^{-\frac{Q_y^2}{2}} \exp \left[\frac{-1}{4} \left([Q_y + w(k_y) - w(k_y - q_y)]^2 + [Q_y + w(k'_y + q_y) - w(k'_y)]^2 \right) \right] \\
& \times \exp \left[i\tau \left(Q_x \left[\frac{2k_y - Q_y + w(k_y) + w(k_y - q_y)}{2} \right] - k_x k_y + [k_x - q_x](k_y - Q_y) \right) \right] \\
& \times \exp \left[i\tau' \left(-Q_x \left[\frac{2k'_y + Q_y + w(k'_y) + w(k'_y + q_y)}{2} \right] - k'_x k'_y + [k'_x + q_x](k'_y + Q_y) \right) \right].
\end{aligned} \tag{77}$$

In Fig. 4d-f, we have used $w(k_y) = f \sin(k_y/Q)$. The effect of the distortion is to induce dispersion in the previously flat bands, as well as to redistribute the exciton Berry curvature. However the bands are still topological for finite f .

Spin-Flip and Valley-Flip Excitons in TBG

In this section, we describe the equations for computing the spin-flip and valley-flip exciton bands in TBG. Our approach is equivalent to diagonalizing in the subspace of single PH pairs in the relevant symmetry sector. We do not consider ‘inter-band’ excitons that are not charged under valley or spin.

We begin with a set of self-consistent Hartree-Fock (HF) band operators $d_{\mathbf{k},\tau\sigma a}^\dagger$ associated with a QAH state |HF⟩ at $\nu = +3$, where τ, σ refer to valley and spin. Since our ‘active’ subspace of the continuum model [21] comprises the eight central bands, the HF band index takes values $a = +, -$. Without loss of generality, we assume that |HF⟩ is flavor polarized such that $d_{\mathbf{k},K'\downarrow+}^\dagger$ is the operator for the single unfilled band. We defer to the Supplementary Materials of Ref [35] for computational details of the continuum model, matrix elements, and HF procedure.

We first focus on intervalley excitons. Following the notation of Ref [36], we parameterize the exciton creation operator at momentum \mathbf{q} as

$$Q_\nu^\dagger(\mathbf{q}) = \sum_{\mathbf{k}a} X_{\mathbf{k}a}^\nu(\mathbf{q}) d_{\mathbf{k}+\mathbf{q},K'\downarrow+}^\dagger d_{\mathbf{k},K\downarrow a} \tag{78}$$

where ν labels the exciton branch. The exciton envelopes $X_{\mathbf{k}a}^\nu(\mathbf{q})$ and energies $\omega_\nu(\mathbf{q})$ are obtained by solving the eigenvalue equation

$$\sum_{\mathbf{k}'a'} A_{\mathbf{k}a;\mathbf{k}'a'}(\mathbf{q}) X_{\mathbf{k}'a}^\nu(\mathbf{q}) = \omega_\nu(\mathbf{q}) X_{\mathbf{k}a}^\nu(\mathbf{q}). \tag{79}$$

The matrix $A_{\mathbf{k}x;\mathbf{k}'y}(\mathbf{q})$ can be split into a ‘single-particle’ and an interaction piece. The single-particle contribution is

$$A_{\mathbf{k}x;\mathbf{k}'y}^{\text{SP}}(\mathbf{q}) = \delta_{\mathbf{k}\mathbf{k}'} (H_{\mathbf{k}+\mathbf{q},K'\downarrow;+\mathbf{q}}^{\text{SP}} \delta_{xy} - H_{\mathbf{k},K\downarrow;y\mathbf{q}}^{\text{SP}}) \tag{80}$$

where the effective single-particle Hamiltonian H^{SP} is off-diagonal only in HF band index. This includes the continuum model Hamiltonian H^{CM} , the external sublattice potential H^Δ , as well as a contribution H^{scr} that accounts for the potential of the filled remote valence bands and subtraction of double-counted interactions relative to a fixed reference density (chosen to correspond to decoupled neutral graphene sheets [26, 35]).

The interaction piece is

$$A_{\mathbf{k}x;\mathbf{k}'y}^{\text{int}}(\mathbf{q}) = \delta_{\mathbf{k}\mathbf{k}'} \sum_{\mathbf{p}a} V_{\mathbf{p}K\downarrow a;\mathbf{k}K\downarrow y}^{\mathbf{p}K\downarrow a;\mathbf{k}K\downarrow y} - \delta_{\mathbf{k}\mathbf{k}'} \delta_{xy} \sum_{\mathbf{p}} V_{\mathbf{k}+\mathbf{q},K'\downarrow+;\mathbf{p}K'\downarrow-}^{\mathbf{k}+\mathbf{q},K'\downarrow+;\mathbf{p}K'\downarrow-} \tag{81}$$

$$+ \delta_{\mathbf{k}\mathbf{k}'} \sum_{\mathbf{p}\tau\sigma a} \left(\delta_{xy} V_{\mathbf{p}\tau\sigma a;\mathbf{k}+\mathbf{q},K'\downarrow+}^{\mathbf{k}+\mathbf{q},K'\downarrow+;\mathbf{p}\tau\sigma a} - V_{\mathbf{p}\tau\sigma a;\mathbf{k}K\downarrow x}^{\mathbf{k}K\downarrow y;\mathbf{p}\tau\sigma a} \right) n_{\tau\sigma a} \tag{82}$$

$$- V_{\mathbf{k}K\downarrow x;\mathbf{k}'+\mathbf{q},K'\downarrow+}^{\mathbf{k}+\mathbf{q},K'\downarrow+;\mathbf{k}'K\downarrow y} \tag{83}$$

where $V_{\gamma;\delta}^{\alpha;\beta} = \langle \alpha; \beta | \hat{V} | \delta; \gamma \rangle$ is the interaction matrix element and $n_{\tau\sigma a}$ is 1 if the band is filled and 0 otherwise. The first line above reflects the loss of exchange energy of the created hole and the gain of exchange energy of the added electron. The second line accounts for the interaction of the PH pair with the filled active bands. The third line describes the mutual interaction of the electron and the hole.

The corresponding expressions for the spin-flip exciton are

$$Q_\nu^\dagger(\mathbf{q}) = \sum_{\mathbf{k}a} X_{\mathbf{k}a}^\nu(\mathbf{q}) d_{\mathbf{k}+\mathbf{q},K'\downarrow}^\dagger d_{\mathbf{k},K'\uparrow a} \quad (84)$$

$$A_{\mathbf{k}x;\mathbf{k}'y}^{\text{SP}}(\mathbf{q}) = \delta_{\mathbf{k}\mathbf{k}'} (H_{\mathbf{k}+\mathbf{q},K'\downarrow;+\mathbf{q}}^{\text{SP}} \delta_{xy} - H_{\mathbf{k},K'\uparrow;yx}^{\text{SP}}) \quad (85)$$

$$A_{\mathbf{k}x;\mathbf{k}'y}^{\text{int}}(\mathbf{q}) = \delta_{\mathbf{k}\mathbf{k}'} \sum_{\mathbf{p}a} V_{\mathbf{p}K'\uparrow a;\mathbf{k}K'\uparrow x}^{\mathbf{p}K'\uparrow a;\mathbf{k}K'\uparrow y} - \delta_{\mathbf{k}\mathbf{k}'} \delta_{xy} \sum_{\mathbf{p}} V_{\mathbf{k}+\mathbf{q},K'\downarrow;+\mathbf{q};\mathbf{p}K'\downarrow-}^{\mathbf{k}+\mathbf{q},K'\downarrow;+\mathbf{q};\mathbf{p}K'\downarrow-} \quad (86)$$

$$+ \delta_{\mathbf{k}\mathbf{k}'} \sum_{\mathbf{p}\tau\sigma a} \left(\delta_{xy} V_{\mathbf{p}\tau\sigma a;\mathbf{k}+\mathbf{q},K'\downarrow+}^{\mathbf{k}+\mathbf{q},K'\downarrow;+\mathbf{q};\mathbf{p}\tau\sigma a} - V_{\mathbf{p}\tau\sigma a;\mathbf{k}K'\uparrow x}^{\mathbf{k}K'\uparrow y;\mathbf{p}\tau\sigma a} \right) n_{\tau\sigma a} \quad (87)$$

$$- V_{\mathbf{k}K'\uparrow x;\mathbf{k}'+\mathbf{q},K'\downarrow+}^{\mathbf{k}+\mathbf{q},K'\downarrow;+\mathbf{q};\mathbf{k}'K'\uparrow y}. \quad (88)$$

Exciton Berry Curvature

In this section, we review how to characterize the curvature [3] and topology of exciton bands. For the sake of notation, it will be useful to recap how it works in standard SP bands. In the discussion below we consider just two SP bands for simplicity. The generalization to multiple filled bands is straightforward. We assume for simplicity that each UC has a finite-orbital basis (indexed by α, β). SP Bloch states are defined

$$|\phi_{\mathbf{k},\tau}\rangle = \sum_{\alpha} u_{\mathbf{k},\tau\alpha} |\mathbf{k}, \alpha\rangle = \frac{1}{\sqrt{N}} \sum_{\mathbf{R},\alpha} u_{\mathbf{k},\tau\alpha} e^{i\mathbf{k}\mathbf{R}} |\mathbf{R}, \alpha\rangle \quad (89)$$

where τ is a band index. We can only compare states with the same boundary conditions [19], so we consider the cell-periodic u 's

$$|u_{\mathbf{k},\tau}\rangle \equiv e^{-i\mathbf{k}\hat{\mathbf{r}}} |\phi_{\mathbf{k},\tau}\rangle = \frac{1}{\sqrt{N}} \sum_{\mathbf{R},\alpha} u_{\mathbf{k},\tau\alpha} |\mathbf{R}, \alpha\rangle. \quad (90)$$

The connection and curvature are then

$$\mathbf{a}_\tau(\mathbf{k}) = -i \sum_{\alpha} u_{\mathbf{k},\tau\alpha}^* \partial_{\mathbf{k}} u_{\mathbf{k},\tau\alpha} \quad (91)$$

$$f_\tau(\mathbf{k}) = \partial_{k_x} a_{\tau,y}(\mathbf{k}) - \partial_{k_y} a_{\tau,x}(\mathbf{k}). \quad (92)$$

This same curvature is probed numerically by evaluating gauge-invariant fluxes [20]

$$f_\tau(\mathbf{k}) \sim \text{Im} \log \langle u_{\mathbf{k},\tau} | u_{\mathbf{k}+\hat{x},\tau} \rangle \langle u_{\mathbf{k}+\hat{x},\tau} | u_{\mathbf{k}+\hat{x}+\hat{y},\tau} \rangle \langle u_{\mathbf{k}+\hat{x}+\hat{y},\tau} | u_{\mathbf{k}+\hat{y},\tau} \rangle \langle u_{\mathbf{k}+\hat{y},\tau} | u_{\mathbf{k},\tau} \rangle, \quad (93)$$

the integral of which is the Chern number. In the case that there are bands that are not completely energetically isolated, the above can be generalized to compute the Chern index of the set of bands [20].

Consider the following exciton wavefunction $|\text{exc}, \mathbf{q}\rangle = \sum_{\mathbf{k}} \tilde{\psi}_{\mathbf{q}}(\mathbf{k}) d_{\mathbf{k}+\mathbf{q},-}^\dagger d_{\mathbf{k},+} |G\rangle$, where $|G\rangle$ consists of a filled + band. There are now two important steps. First, we perform a particle-hole transformation in the $\tau = -$ band so that we can work with two-particle states. Second, we need to be careful about CM and relative decomposition. The point is that the CM momentum should be defined in order to properly couple to the CM position $\mathbf{R} = \frac{\mathbf{r}_1 + \mathbf{r}_2}{2}$. Therefore we define the exciton state as

$$|\psi_{\mathbf{q}}^{\text{exc}}\rangle = \sum_{\mathbf{k}} \psi_{\mathbf{q}}(\mathbf{k}) |\phi_{\mathbf{k}+\frac{\mathbf{q}}{2},-}\rangle |\phi_{\mathbf{k}-\frac{\mathbf{q}}{2},+}^*\rangle \quad (94)$$

where $\psi_{\mathbf{q}}(\mathbf{k}) = \tilde{\psi}_{\mathbf{q}}(\mathbf{k} - \frac{\mathbf{q}}{2})$. Now for a finite-orbital basis

$$|\psi_{\mathbf{q}}^{\text{exc}}\rangle = \sum_{\mathbf{k}} \psi_{\mathbf{q}}(\mathbf{k}) \sum_{\alpha\beta\mathbf{r}_1\mathbf{r}_2} u_{\mathbf{k}+\frac{\mathbf{q}}{2},-\alpha} u_{\mathbf{k}-\frac{\mathbf{q}}{2},+\beta}^* e^{i(\mathbf{k}+\frac{\mathbf{q}}{2})\mathbf{r}_1} e^{-i(\mathbf{k}-\frac{\mathbf{q}}{2})\mathbf{r}_2} |\mathbf{r}_1, \alpha\rangle |\mathbf{r}_2, \beta\rangle \quad (95)$$

$$|u_{\mathbf{q}}^{\text{exc}}\rangle \equiv e^{-i\mathbf{q}(\frac{\mathbf{r}_1 + \mathbf{r}_2}{2})} |\psi_{\mathbf{q}}^{\text{exc}}\rangle = \sum_{\mathbf{k}} \psi_{\mathbf{q}}(\mathbf{k}) \sum_{\alpha\beta\mathbf{r}_1\mathbf{r}_2} u_{\mathbf{k}+\frac{\mathbf{q}}{2},-\alpha} u_{\mathbf{k}-\frac{\mathbf{q}}{2},+\beta}^* e^{i\mathbf{k}(\mathbf{r}_1 - \mathbf{r}_2)} |\mathbf{r}_1, \alpha\rangle |\mathbf{r}_2, \beta\rangle, \quad (96)$$

where the u 's are defined so that they have the same CM boundary conditions for different \mathbf{q} . Hence a sensible connection can be defined analogously to the single-particle case

$$\mathbf{a}^{\text{exc}}(\mathbf{q}) \equiv -i \langle u_{\mathbf{q}}^{\text{exc}} | \partial_{\mathbf{q}} | u_{\mathbf{q}}^{\text{exc}} \rangle \quad (97)$$

$$= -i \sum_{\mathbf{k}} \psi_{\mathbf{q}}^*(\mathbf{k}) \partial_{\mathbf{q}} \psi_{\mathbf{q}}(\mathbf{k}) + \frac{1}{2} \sum_{\mathbf{k}} |\psi_{\mathbf{q}}(\mathbf{k})|^2 a_{-}(\mathbf{k} + \frac{\mathbf{q}}{2}) + \frac{1}{2} \sum_{\mathbf{k}} |\psi_{\mathbf{q}}(\mathbf{k})|^2 a_{+}(\mathbf{k} - \frac{\mathbf{q}}{2}). \quad (98)$$

The exciton curvature is

$$f^{\text{exc}}(\mathbf{q}) \equiv \partial_{q_x} a_y^{\text{exc}}(\mathbf{q}) - \partial_{q_y} a_x^{\text{exc}}(\mathbf{q}) \quad (99)$$

$$= -i \sum_{\mathbf{k}} \left[(\partial_{q_x} \psi_{\mathbf{q}}^*(\mathbf{k})) (\partial_{q_y} \psi_{\mathbf{q}}(\mathbf{k})) - (\partial_{q_y} \psi_{\mathbf{q}}^*(\mathbf{k})) (\partial_{q_x} \psi_{\mathbf{q}}(\mathbf{k})) \right] \quad (100)$$

$$+ \frac{1}{4} \sum_{\mathbf{k}} |\psi_{\mathbf{q}}(\mathbf{k})|^2 f_{-}(\mathbf{k} + \frac{\mathbf{q}}{2}) - \frac{1}{4} \sum_{\mathbf{k}} |\psi_{\mathbf{q}}(\mathbf{k})|^2 f_{+}(\mathbf{k} - \frac{\mathbf{q}}{2}) \quad (101)$$

$$+ \frac{1}{2} \sum_{\mathbf{k}} \left[(\partial_{q_x} |\psi_{\mathbf{q}}(\mathbf{k})|^2) (a_{-,y}(\mathbf{k} + \frac{\mathbf{q}}{2})) + (\partial_{q_x} |\psi_{\mathbf{q}}(\mathbf{k})|^2) (a_{+,y}(\mathbf{k} - \frac{\mathbf{q}}{2})) - (x \leftrightarrow y) \right] \quad (102)$$

It can be verified that the curvature is gauge-invariant under the following transforms

$$|\phi_{\mathbf{k},-}\rangle \rightarrow e^{i\varphi_{-}(\mathbf{k})} |\phi_{\mathbf{k},-}\rangle \quad (103)$$

$$|\phi_{\mathbf{k},+}\rangle \rightarrow e^{i\varphi_{+}(\mathbf{k})} |\phi_{\mathbf{k},+}\rangle \quad (104)$$

$$\psi_{\mathbf{q}}(\mathbf{k}) \rightarrow e^{i(\varphi_{+}(\mathbf{k}-\frac{\mathbf{q}}{2})-\varphi_{-}(\mathbf{k}+\frac{\mathbf{q}}{2}))} e^{i\theta(\mathbf{q})} \psi_{\mathbf{q}}(\mathbf{k}). \quad (105)$$

Numerically the curvature is probed by evaluating gauge-invariant loops, similarly to the SP case

$$f(\mathbf{k}) \sim \text{Im} \log \langle u_{\mathbf{k}}^{\text{exc}} | u_{\mathbf{k}+\hat{z}}^{\text{exc}} \rangle \langle u_{\mathbf{k}+\hat{z}}^{\text{exc}} | u_{\mathbf{k}+\hat{1}+\hat{z}}^{\text{exc}} \rangle \langle u_{\mathbf{k}+\hat{1}+\hat{z}}^{\text{exc}} | u_{\mathbf{k}+\hat{1}}^{\text{exc}} \rangle \langle u_{\mathbf{k}+\hat{1}}^{\text{exc}} | u_{\mathbf{k}}^{\text{exc}} \rangle. \quad (106)$$